JACS
JOURNAL OF THE AMERICAN CHEMICAL SOCIETY
pubs.acs.org/JACS
Communication

# $[Cu_4@E_{18}]^{4-}$ (E = Sn, Pb): Fused Derivatives of Endohedral Stannaspherene and Plumbaspherene

Lei Qiao,[§] Chao Zhang,[§] Cong-Cong Shu,[§] Harry W. T. Morgan, John E. McGrady,* and Zhong-Ming Sun*

Cite This: J. Am. Chem. Soc. 2020, 142, 13288−13293
Read Online



**ABSTRACT:** We report the synthesis of two new cluster anions, $[Cu_4@E_{18}]^{4-}$ (E = Sn, Pb), in which a $Cu_4$ subunit is incorporated into a continuous $E_{18}$ tetrel cage. Both anions are characterized by X-ray crystallography and mass spectrometry, complemented by quantum-chemical calculations that highlight the relationships to known Zintl clusters, including the stannaspherenes and plumbaspherenes $[M@Sn_{12}]^{q-}$ and $[M@Pb_{12}]^{q-}$, the Matryoshka bronze $[Sn@Cu_{12}@Sn_{20}]^{12-}$, and also $[Pd_2@E'_{18}]^{4-}$ (E′ = Ge, Sn).



The icosahedral inorganic fullerene analogues stannaspherene ($[Sn_{12}]^{2-}$) and plumbaspherene ($[Pb_{12}]^{2-}$) were first characterized in the gas phase by Wang and co-workers in 2006,[1−4] and they have been shown to encapsulate a range of transition metal ions. For example, $[Ir@Sn_{12}]^{3-}$ and $[M@Pb_{12}]^{q-}$ (M = Ni, Pd, Pt, $q$ = 2; M = Co, Rh, Ir, $q$ = 3) have all now been characterized in the solid state, and all retain an almost perfectly icosahedral cage.[5,6] Substantial distortions of the icosahedron are apparent in cases such as $[Co@Ge_{12}]^{3-}$, $[Mn@Pb_{12}]^{3-}$, and $[Rh@Sn_{12}]^{3-}$,[7−9] and even completely nondeltahedral geometries are known, for example in $D_{2d}$-symmetric $[Ru@Ge_{12}]^{3-}$.[10] The relationship between structure and electron count in these 12-vertex clusters has been explored using density functional theory.[11] Smaller 10-vertex clusters, including bicapped square-antiprismatic $[Ni@Pb_{10}]^{2-}$ and pentagonal-prismatic $[M@Ge_{10}]^{3-}$ (M = Fe, Co), are also known,[12−14] as are nine-vertex $[Cu@E_9]^{3-}$ (E = Sn, Pb), $[Ni@Sn_9]^{4-}$, $[Co@Ge_9]^{5-}$, and $[Ru@Sn_9]^{6-}$.[15−17] In contrast, clusters containing multiple transition metal atoms are rather less common, although recent examples include $[Co_2@Ge_{16}]^{4-}$ (Figure 1A),[18] $[M_2@Sn_{17}]^{q-}$ (M = Ni, Pt, $q$ = 4;[19,20] Co, $q$ = 5[21]) (Figure 1B), $[Pd_2@E'_{18}]^{4-}$ (E′ = Ge, Sn) (Figure 1C),[22] $[Rh_3@Sn_{24}]^{5-}$ (Figure 1D),[8] and $[Ni_3@Ge_{18}]^{4-}$ and $[Pd_3@Sn_8Bi_6]^{4-}$ (Figure 1E).[23,24] The chemistry of these and other Zintl clusters has been the subject of a number of recent reviews.[25] Of particular relevance to this work is the so-called "Matryoshka bronze" cluster, $[Sn@Cu_{12}@Sn_{20}]^{12-}$ (Figure 1F), which contains a Sn atom encapsulated by a $Cu_{12}$ icosahedron that is in turn encapsulated by a $Sn_{20}$ pentagonal dodecahedron.[26] The notion that molecular clusters represent an embryonic form of the metallic state is now well-established,[27] and recent developments in Cu/Zn cluster chemistry have shed important light on the evolution of "embryonic brass".[28] While the Cu:Sn ratio of 4:7 in $[Sn@Cu_{12}@Sn_{20}]^{12-}$ is much lower than in typical bronzes (∼12% Sn), it is close to that in the intermetallic $Cu_6Sn_5$ phase, and the clear segregation of Cu and Sn content provides important molecular-level insights into the factors that control the alloying process. In this paper, we report a new member of the binary Cu/Sn cluster family, $[Cu_4@Sn_{18}]^{4-}$, along with its lead analogue, $[Cu_4@Pb_{18}]^{4-}$ (Figures 2A,B, S2, and S3). Both clusters contain a continuous $D_{2h}$-symmetric $Sn_{18}/Pb_{18}$ cage with the four Cu atoms arranged in a rhombus. The Cu:E ratio of 2:9 is even lower than in the Matryoshka bronze, offering an opportunity to explore how the interactions between the Cu and tetrel components of binary clusters evolve as a function of composition. We also explore the structural and electronic relationship between $[Cu_4@E_{18}]^{4-}$ and the known palladium analogues $[Pd_2@E'_{18}]^{4-}$, which also have a continuous 18-

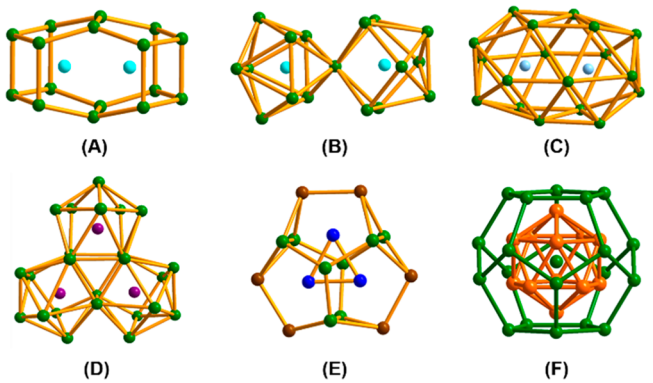


**Figure 1.** Structures of selected endohedral clusters with more than one metal: (A) α-$[Co_2@Ge_{16}]^{4-}$; (B) $[M_2@Sn_{17}]^{q-}$ (M = Ni, $q$ = 4; Co, $q$ = 5); (C) $[Pd_2@E'_{18}]^{4-}$ (E′ = Ge, Sn); (D) $[Rh_3@Sn_{24}]^{5-}$; (E) $[Pd_3@Sn_8Bi_6]^{4-}$; (F) $[Sn@Cu_{12}@Sn_{20}]^{12-}$.

**Received:** May 5, 2020
**Published:** July 21, 2020




https://dx.doi.org/10.1021/jacs.0c04815
J. Am. Chem. Soc. 2020, 142, 13288−13293

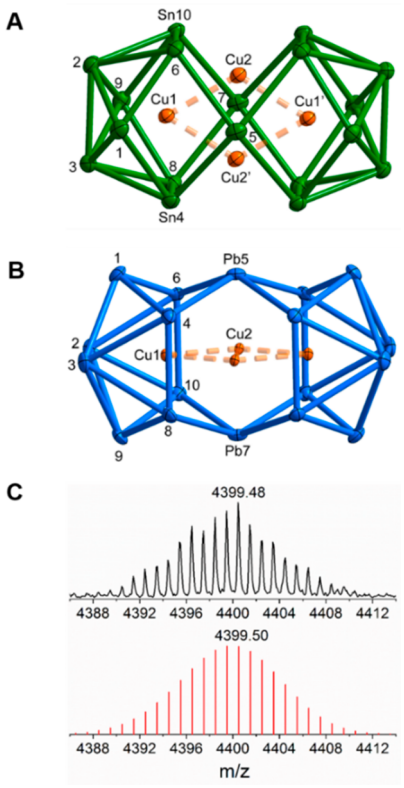


**Figure 2.** (A, B) ORTEP representations of (A) $[Cu_4@Sn_{18}]^{4-}$ viewed down the *x* axis and (B) $[Cu_4@Pb_{18}]^{4-}$ viewed down the *y* axis. Thermal ellipsoids are drawn at 75% probability in both cases. The two clusters are isostructural. (C) ESI(−) mass peak corresponding to $[K(2.2.2\text{-crypt})Cu_4Pb_{18}]^-$. The experimental mass distributions are depicted in black, and the theoretical masses of the isotope distributions are shown in red.

vertex tetrel cage but a more highly fused structure (Figure 1C).

The title compounds, $[K(2.2.2\text{-crypt})]_4[Cu_4@E_{18}]\cdot 4DMF$ (E = Sn, Pb), were both prepared by the reaction of an ethylenediamine (en) solution of $K_4E_9$ with $Cu_4Mes_4(THT)_2$[29] (detailed syntheses are listed in the Supporting Information). The electrospray ionization (ESI) mass spectra of **2** reveal the presence of relatively strong peaks attributable to $[K(2.2.2\text{-crypt})Cu_4Pb_{18}]^-$ (Figure 2C). Single-crystal X-ray diffraction indicates that both **1** and **2** crystallize in the $P\bar{1}$ space group with four $[K(2.2.2\text{-crypt})]^+$ cations and four DMF molecules in the corresponding unit cell. The structures of $[Cu_4@Sn_{18}]^{4-}$ and $[Cu_4@Pb_{18}]^{4-}$ are shown (from two different perspectives) in Figure 2; it should be noted that the two clusters are isostructural. The 18-vertex tin or lead cage is made up of two $E_{10}$ "sphenocorona" fused along a common edge (E5−E7 in Figure 3), giving an approximately

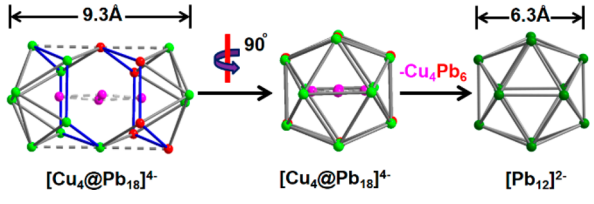


**Figure 3.** Structural relationship between $[Cu_4@Pb_{18}]^{4-}$ and $[Pb_{12}]^{2-}$.

$D_{2h}$-symmetric structure with 2-fold rotational axes along the Cu2−Cu2′, Cu1−Cu1′, and E5-E7 vectors. When viewed along the prolate (*z*) axis (Cu1−Cu1′), the dimensions of the cluster are strikingly similar to those of the icosahedral $[E_{12}]^{2-}$ anions (Figure 3), which have diameters of 6.3 and 6.1 Å, respectively. The $E_{18}$ cage can be derived, at least conceptually, by inserting a chairlike $E_6$ unit (shown in red in Figure 3) between one triangular face of an icosahedron and the remaining $E_9$ fragment. In that sense, the title compounds can be viewed as fused analogues of the icosahedral parents, stannaspherene and plumbaspherene. The Cu atoms are found in two distinct coordination environments: Cu1 and Cu1′ lie approximately at the foci of the "$E_{10}$ subunits" and have short Cu−E distances to ten E atoms. Cu2 and Cu2′, in contrast, lie outside the body of the $E_{18}$ cluster and are coordinated by only six E atoms in a trigonal-prismatic array. The four Cu−Cu distances around the circumference of the rhombus (Cu1−Cu2) in **1** are in the range 2.5292(12)−2.5511(13) Å, comparable to that in $\{[CuGe_9Mes]_2\}^{4-}$ (2.5214(7) Å),[30] while the diagonal Cu2−Cu2′ distance is 2.6302(12) Å. These values are significantly shorter than those in $[Sn@Cu_{12}@Sn_{20}]^{12-}$, where all 20 Cu−Cu distances are ∼2.79 Å. The bonded Cu−Sn distances of 2.6730(19)−2.8415(27) Å in **1** are slightly shorter than those in $\{[CuSn_5Sb_3]^{2-}\}_2$ (2.753(2)−2.961(2) Å) but somewhat longer than those in tricapped trigonal-prismatic $[Cu@Sn_9]^{3-}$ (2.611(7)−2.700(7) Å), $[Sn@Cu_{12}@Sn_{20}]^{12-}$ (2.631(1)−2.796(1) Å), and $[NHC^{Dipp}Cu(\eta^4\text{-}Sn_9)]^{3-}$ (2.7216(7)-2.7491(7) Å) and in the Cu−Sn intermetallic phases $Na_{12}Cu_{12}Sn_{21}$, $Ca_3Cu_8Sn_4$, $CaCu_9Sn_4$, and $Ca_6Cu_2Sn_7$ (2.585(1)−2.869(1) Å).[31]

Given the similarity, at least in terms of elemental composition, between $[Cu_4@Sn_{18}]^{4-}$ and the Matryoshka bronze, $[Sn@Cu_{12}@Sn_{20}]^{12-}$, it is useful to compare the electronic structures of the two clusters to see whether the different stoichiometries and structures reflect substantial differences in the element−element bonding. To make this comparison, we turned to density functional theory (all of the calculations were performed using ADF2019.103[32−34] with the PBE functional[35] and a polarized triple-ζ basis set—full details are given in the Supporting Information). The idealized $D_{2h}$-symmetric structure that emerges from the X-ray analysis proves to be a local minimum on the potential energy surface of $[Cu_4@Sn_{18}]^{4-}$. Full details of the Cartesian coordinates are given in section 5 in the Supporting Information, and the optimized bond lengths are presented in Tables S2 and S3 alongside the X-ray data. The optimized Cu−Cu and Cu−Sn separations are within 2% of the experimentally determined values, but the Sn−Sn bond lengths are overestimated by ∼0.1 Å, a typical observation in calculations on highly anionic Zintl clusters that probably stems from the absence of an explicit cationic environment in the computational model. Nevertheless, it is clear that the computational model captures the essential geometric features of these clusters. The projected density of states for $[Cu_4@Sn_{18}]^{4-}$ is presented in Figure 4, alongside that for $[Sn@Cu_{12}@Sn_{20}]^{12-}$. The latter is qualitatively identical to that reported previously by Stegmaier and Fässler.[26] In both cases, the discrete energy levels are broadened using a Lorentzian line shape (fwhm = 0.1 eV), and the zero of energy is taken as the midpoint of the HOMO−LUMO gap. The principal features of the densities of states for the two clusters are strikingly similar. The highest occupied orbitals are dominated by Sn 5p character (green), with a narrow band of predominantly Cu 3d orbitals (orange)


https://dx.doi.org/10.1021/jacs.0c04815
J. Am. Chem. Soc. 2020, 142, 13288−13293

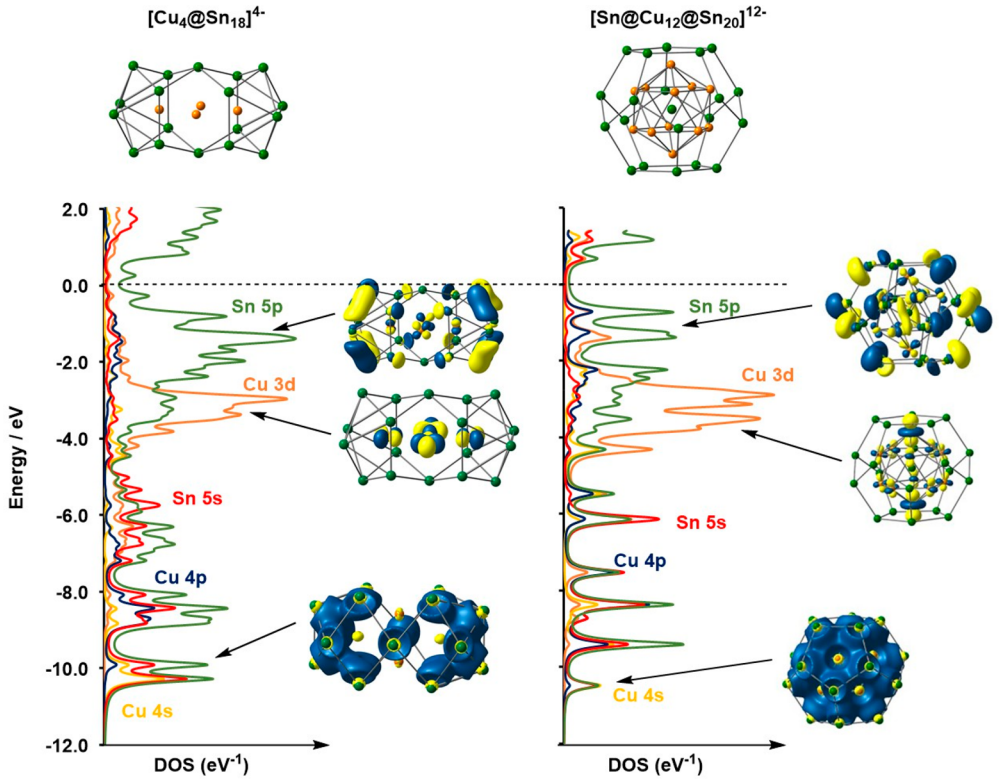


**Figure 4.** Comparison of the densities of states for $[Cu_4@Sn_{18}]^{4-}$ and $[Sn@Cu_{12}@Sn_{20}]^{12-}$. Eigenvalues are broadened with a Lorentzian line shape with a full width at half-maximum of 0.1 eV. Representative orbitals from each region are also shown.

approximately 3 eV below the HOMO. Below that lies a broad band of orbitals dominated by Sn 5s character (red) mixed with some Cu 4s and 4p. The Cu 3d band is completely filled in both clusters, suggesting that significant Cu−Cu bonding is absent, despite the short Cu−Cu distances in $[Cu_4@Sn_{18}]^{4-}$. The relative heights of the Cu 3d and Sn 5p bands reflect the differing stoichiometries of the two clusters, but the otherwise striking similarities between the two plots suggest that the Cu−Sn interactions do not differ greatly despite the clear differences in composition and structure.

The very different coordination geometries of the two symmetry-distinct Cu sites (Cu1 and Cu2) in $[Cu_4@E_{18}]^{4-}$ suggest that they may play rather different roles in stabilizing the cluster. The Cu2 atoms lie outside the body of the $E_{18}$ cluster and in that sense are reminiscent of the "tightly bound" alkali metal ions in highly charged Zintl anions such as $K_{12}[Sn@Cu_{12}@Sn_{20}]$ and $[K_3Rh_2Sn_{17}]^{3-}$.[9] Consistent with this idea, we find that if we remove the Cu2 centers as cations, the naked $[Cu_2@Sn_{18}]^{6-}$ anion relaxes to a local minimum with bond lengths and angles that are largely unchanged from those in $[Cu_4@Sn_{18}]^{4-}$ (Figure 5). The frontier orbitals are also largely unchanged by the removal of the two $Cu^+$ ions. Moreover, if we replace $Cu^+$ ions in the Cu2 sites with $K^+$ (which is present in abundance in the reaction solution and thus could in principle occupy these sites), the $K^+$ ions are expelled from the cluster: clearly they are ill-suited to the role of charge compensation because they are too large to fit in the interstitial cavities occupied by Cu2. All of the above results suggest that the principal role of the ions in the Cu2 sites is to stabilize the high negative charge and that they are not integral to the structure of the cluster. The formulation of **1** and **2** as $(Cu^+)_2[Cu_2@E_{18}]^{6-}$ allows for a direct comparison to the known $[Pd_2@E'_{18}]^{4-}$ anions, which also have a continuous 18-vertex tetrel cage, albeit one with $D_{3d}$ rather than $D_{2h}$ symmetry (Figure 5).[22] The valence electron counts of $[Cu_2@Sn_{18}]^{6-}$ and $[Pd_2@Sn_{18}]^{4-}$ are 80 and 76, respectively, and a reduction in electron count in cluster chemistry is typically associated with depopulation of antibonding orbitals and hence the formation of additional bonds (the comparison of $S_8$ and $S_8^{2+}$ is a classic case).[36] If four electrons are removed from $[Cu_2@Sn_{18}]^{6-}$ to generate 76-electron $[Cu_2@Sn_{18}]^{2-}$, the cluster relaxes to a $D_{3d}$-symmetric minimum with additional trans-equatorial bonds (Sn4−Sn8′ and Sn6−Sn10′ in Figure 5), isostructural with $[Pd_2@Sn_{18}]^{4-}$. The four electrons are removed from orbitals that are antibonding across the equator of the cluster ($19a_{2u}$ and one component of $25e_g$ in Figure 5, right). This orbital correlation diagram establishes a conceptual link between the structures of $[Cu_4@Sn_{18}]^{4-}$, where the two $M@Sn_9$ hemispheres are rather loosely connected across the equator, and $[Pd_2@Sn_{18}]^{4-}$, where they are more tightly fused. Dehnen and co-workers have argued that cluster growth occurs through the fusion of small preformed fragments,[37] and the link between the $D_{2h}$- and $D_{3d}$-symmetric isomers of the $E_{18}$ cage allows us to speculate on possible pathways that lead to the $M_xE_{18}$ cluster family. On the basis of the well-established stability of $[Cu@Sn_9]^{3-}$,[15] a dimerization leading to $[Cu_2@Sn_{18}]^{6-}$ seems plausible, with the substantial Coulomb repulsion that this entails being buffered by the binding of two $Cu^+$ ions in the Cu2 sites. Alternatively, it is possible that binding of $Cu^+$ to $[Cu@Sn_9]^{3-}$ precedes dimerization. In cases where trapped ions are more reducible than $Cu^+$ ($Pd^{2+}$, for example), we can envisage that they might act as vehicles to remove excess electron density from the cluster, forming elemental metal along with additional Sn−Sn bonds. The fusion of cluster fragments with simultaneous trapping of charge-compensating cations, followed by reductive elimina-


https://dx.doi.org/10.1021/jacs.0c04815
J. Am. Chem. Soc. 2020, 142, 13288−13293

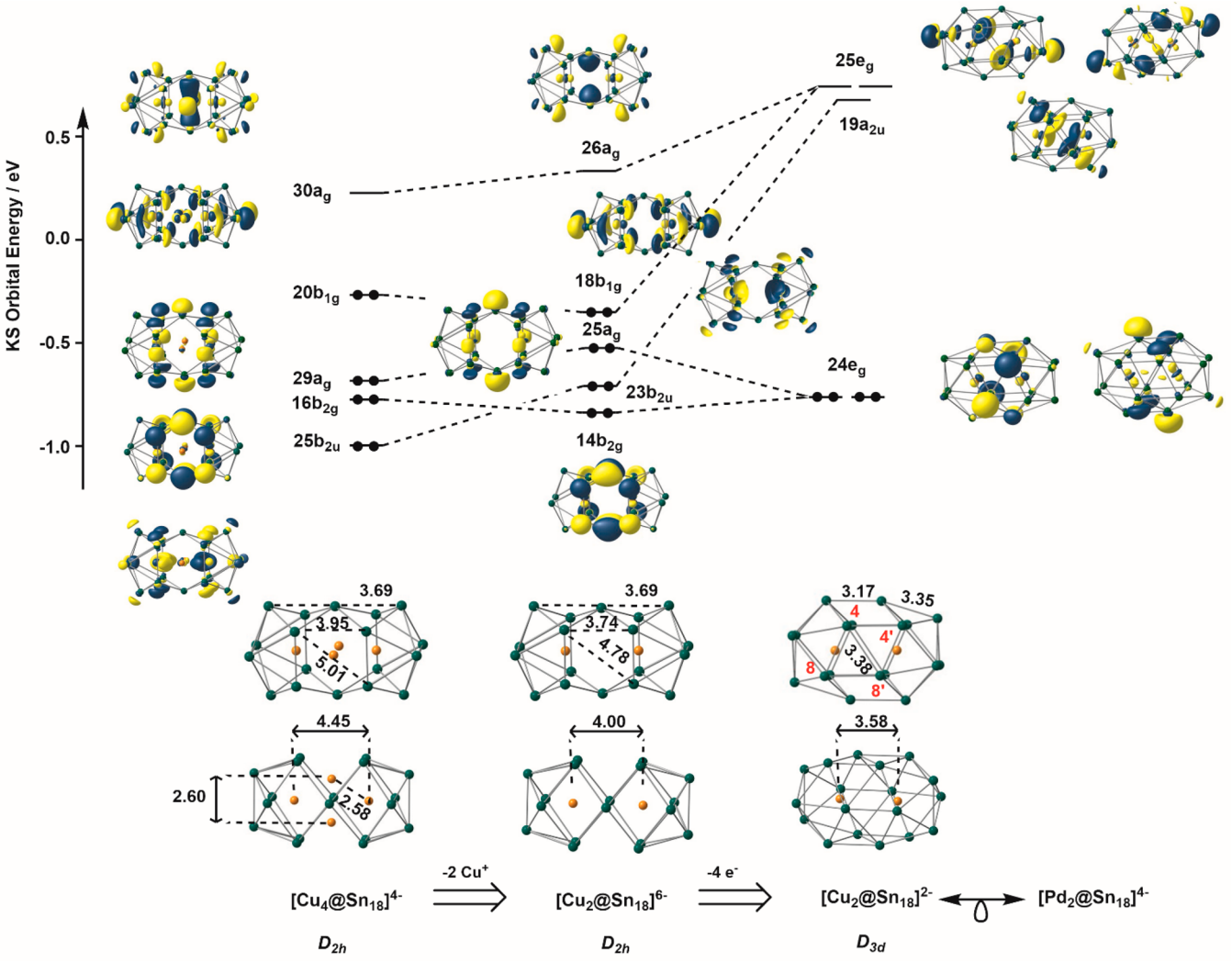


**Figure 5.** Comparison of the structures and frontier Kohn–Sham orbitals of $D_{2h}$-symmetric $[Cu_2@Sn_{18}]^{6-}$ and $D_{3d}$-symmetric $[Cu_2@Sn_{18}]^{2-}$ viewed down the conserved $C_2$ axis. The middle of the HOMO–LUMO gap is taken as the zero of energy for all three clusters.

tion with concomitant E–E bond formation, offers a possible low-energy pathway that avoids the Coulomb explosion associated with fusion of highly anionic moieties.

In summary, we have reported here the synthesis and characterization of two clusters with a continuous 18-vertex, $D_{2h}$-symmetric Sn/Pb cage, $[Cu_4@E_{18}]^{4-}$. The electronic structure of $[Cu_4@Sn_{18}]^{4-}$ is qualitatively similar to the icosahedral Matryoshka bronze, $[Sn@Cu_{12}@Sn_{20}]^{12-}$, despite the obvious differences in Cu:Sn ratio and geometry, suggesting that element–element interactions within the Cu/Sn cluster family are not strongly dependent on the composition. Preliminary results indicate that these $[Cu_4@E_{18}]^{4-}$ clusters loaded on catalyst supports show promising activity in the catalytic reduction of $CO_2$. This observation may be related to the ability of the cluster to tolerate large fluctuations in redox state with only relatively minor changes in structure. Further study of this and related catalytic activity is ongoing.

## ■ ASSOCIATED CONTENT

### Supporting Information

The Supporting Information is available free of charge at https://pubs.acs.org/doi/10.1021/jacs.0c04815.

Detailed experimental procedures, crystallographic supplementation, electrospray ionization mass spectrometry (ESI-MS) analysis, energy-dispersive X-ray (EDX) spectroscopic analysis, and quantum-chemical studies (PDF)

Crystallographic data for **1** (CIF)

Crystallographic data for **2** (CIF)

## ■ AUTHOR INFORMATION


### Corresponding Authors

**Zhong-Ming Sun** – *Tianjin Key Lab for Rare Earth Materials and Applications, State Key Laboratory of Elemento-Organic Chemistry, School of Materials Science and Engineering, Nankai University, Tianjin 300350, China;* orcid.org/0000-0003-2894-6327; Email: sunlab@nankai.edu.cn

**John E. McGrady** – *Department of Chemistry, University of Oxford, Oxford OX1 3QR, U.K.;* orcid.org/0000-0002-8991-1921; Email: john.mcgrady@chem.ox.ac.uk

### Authors

**Lei Qiao** – *Tianjin Key Lab for Rare Earth Materials and Applications, State Key Laboratory of Elemento-Organic Chemistry, School of Materials Science and Engineering, Nankai*




https://dx.doi.org/10.1021/jacs.0c04815
J. Am. Chem. Soc. 2020, 142, 13288–13293

*University, Tianjin 300350, China;* orcid.org/0000-0002-6602-6532

**Chao Zhang** − *Tianjin Key Lab for Rare Earth Materials and Applications, State Key Laboratory of Elemento-Organic Chemistry, School of Materials Science and Engineering, Nankai University, Tianjin 300350, China;* orcid.org/0000-0002-0368-0801

**Cong-Cong Shu** − *Tianjin Key Lab for Rare Earth Materials and Applications, State Key Laboratory of Elemento-Organic Chemistry, School of Materials Science and Engineering, Nankai University, Tianjin 300350, China;* orcid.org/0000-0001-7407-3446

**Harry W. T. Morgan** − *Department of Chemistry, University of Oxford, Oxford OX1 3QR, U.K.;* orcid.org/0000-0001-9647-8807

Complete contact information is available at: https://pubs.acs.org/10.1021/jacs.0c04815

### Author Contributions

[§]L.Q., C.Z., and C.-C.S. contributed equally.

### Notes

The authors declare no competing financial interest.

## ■ ACKNOWLEDGMENTS

This work was supported by the National Natural Science Foundation of China (21971118 and 21722106 to Z.-M.S.). H.W.T.M. thanks the EPSRC for support through the Centre for Doctoral Training, Theory and Modelling in Chemical Sciences under Grant EP/L015722/1.

## ■ REFERENCES

(1) Cui, L. F.; Huang, X.; Wang, L. M.; Zubarev, D. Y.; Boldyrev, A. I.; Li, J.; Wang, L. S. $Sn_{12}^{2-}$: Stannaspherene. *J. Am. Chem. Soc.* **2006**, *128*, 8390−8391.

(2) Cui, L. F.; Huang, X.; Wang, L. M.; Li, J.; Wang, L. S. $Pb_{12}^{2-}$: Plumbaspherene. *J. Phys. Chem. A* **2006**, *110*, 10169−10172.

(3) Cui, L. F.; Wang, L. S. Stable Icosahedral Hollow Cage Clusters: Stannaspherene ($Sn_{12}^{2-}$) and Plumbaspherene ($Pb_{12}^{2-}$). *Int. Rev. Phys. Chem.* **2008**, *27*, 139−166.

(4) Cui, L. F.; Huang, X.; Wang, L. M.; Li, J.; Wang, L. S. Endohedral Stannaspherenes $M@Sn_{12}^{-}$: A Rich Class of Stable Molecular Cage Clusters. *Angew. Chem., Int. Ed.* **2007**, *46*, 742−745.

(5) Wang, J. Q.; Stegmaier, S.; Wahl, B.; Fässler, T. F. Step-by-Step Synthesis of the Endohedral Stannaspherene $[Ir@Sn_{12}]^{3-}$ via the Capped Cluster Anion $[Sn_9Ir(cod)]^{3-}$. *Chem. - Eur. J.* **2010**, *16*, 1793−1798.

(6) (a) Esenturk, E. N.; Fettinger, J.; Lam, Y. F.; Eichhorn, B. W. $[Pt@Pb_{12}]^{2-}$. *Angew. Chem., Int. Ed.* **2004**, *43*, 2132−2134. (b) Esenturk, E. N.; Fettinger, J.; Eichhorn, B. W. The $Pb_{12}^{2-}$ and $Pb_{10}^{2-}$ Zintl Ions and the $M@Pb_{12}^{2-}$ and $M@Pb_{10}^{2-}$ Cluster Series Where M = Ni, Pd, Pt. *J. Am. Chem. Soc.* **2006**, *128*, 9178−9186. (c) Li, A. M.; Wang, Y.; Downing, D. O.; Chen, F.; Zavalij, P.; Muñoz-Castro, A.; Eichhorn, B. W. Endohedral Plumbaspherenes of the Group 9 Metals: Synthesis, Structure and Properties of the $[M@Pb_{12}]^{3-}$ (M = Co, Rh, Ir) Ions. *Chem. - Eur. J.* **2020**, *26*, 5824−5833.

(7) Liu, C.; Li, L. J.; Popov, I. A.; Wilson, R. J.; Xu, C. Q.; Li, J.; Boldyrev, A. I.; Sun, Z.-M. Symmetry Reduction upon Size Mismatch: The Non-Icosahedral Intermetalloid Cluster $[Co@Ge_{12}]^{3-}$. *Chin. J. Chem.* **2018**, *36*, 1165−1168.

(8) Zhou, B. B.; Krämer, T.; Thompson, A. L.; McGrady, J. E.; Goicoechea, J. M. A Highly Distorted Open-Shell Endohedral Zintl Cluster: $[Mn@Pb_{12}]^{3-}$. *Inorg. Chem.* **2011**, *50*, 8028−8037.

(9) Liu, C.; Jin, X.; Li, L. J.; Xu, J.; McGrady, J. E.; Sun, Z.-M. Synthesis and Structure of a Family of Rhodium Polystannide Clusters $[Rh@Sn_{10}]^{3-}$, $[Rh@Sn_{12}]^{3-}$, $[Rh_2@Sn_{17}]^{6-}$ and the First Triply-fused Stannide, $[Rh_3@Sn_{24}]^{5-}$. *Chem. Sci.* **2019**, *10*, 4394−4401.

(10) Espinoza-Quintero, G.; Duckworth, J. C. A.; Myers, W. K.; McGrady, J. E.; Goicoechea, J. M. Synthesis and Characterization of $[Ru@Ge_{12}]^{3-}$: An Endohedral 3-Connected Cluster. *J. Am. Chem. Soc.* **2014**, *136*, 1210−1213.

(11) Goicoechea, J. M.; McGrady, J. E. On the Structural Landscape in Endohedral Silicon and Germanium Clusters, $M@Si_{12}$ and $M@Ge_{12}$. *Dalton Trans.* **2015**, *44*, 6755−6766.

(12) Esenturk, E. N.; Fettinger, J.; Eichhorn, B. W. The *closo*-$Pb_{10}^{2-}$ Zintl Ion in the $[Ni@Pb_{10}]^{2-}$ Cluster. *Chem. Commun.* **2005**, 247−249.

(13) Wang, J. Q.; Stegmaier, S.; Fässler, T. F. $[Co@Ge_{10}]^{3-}$: An Intermetalloid Cluster with Archimedean Pentagonal Prismatic Structure. *Angew. Chem.* **2009**, *121*, 2032−2036.

(14) Zhou, B. B.; Denning, M. S.; Kays, D. L.; Goicoechea, J. M. Synthesis and Isolation of $[Fe@Ge_{10}]^{3-}$: A Pentagonal Prismatic Zintl Ion Cage Encapsulating an Interstitial Iron Atom. *J. Am. Chem. Soc.* **2009**, *131*, 2802−2803.

(15) Scharfe, S.; Fässler, T. F.; Stegmaier, S.; Hoffmann, S. D.; Ruhland, K. $[Cu@Sn_9]^{3-}$ and $[Cu@Pb_9]^{3-}$: Intermetalloid Clusters with Endohedral Cu Atoms in Spherical Environments. *Chem. - Eur. J.* **2008**, *14*, 4479−4483.

(16) (a) Rios, D.; Gillett-Kunnath, M. M.; Taylor, J. D.; Oliver, A. G.; Sevov, S. C. Addition of a Thallium Vertex to Empty and Centered Nine-Atom Deltahedral Zintl Ions of Germanium and Tin. *Inorg. Chem.* **2011**, *50*, 2373−2377. (b) Kocak, F. S.; Downing, D. O.; Zavalij, P.; Lam, Y. F.; Vedernikov, A. N.; Eichhorn, B. W. Surprising Acid/Base and Ion-Sequestration Chemistry of $Sn_9^{4-}$: $HSn_9^{3-}$, $Ni@HSn_9^{3-}$, and the $Sn_9^{3-}$ Ion Revisited. *J. Am. Chem. Soc.* **2012**, *134*, 9733−9740.

(17) Witzel, B. J. L.; Klein, W.; Dums, J. V.; Boyko, M.; Fässler, T. F. Metallocages for Metal Anions: Highly Charged $[Co@Ge_9]^{5-}$ and $[Ru@Sn_9]^{6-}$ Clusters Featuring Spherically Encapsulated $Co^{1-}$ and $Ru^{2-}$ Anions. *Angew. Chem., Int. Ed.* **2019**, *58*, 12908−12913.

(18) Liu, C.; Popov, I. A.; Li, L. J.; Li, N.; Boldyrev, A. I.; Sun, Z.-M. $[Co_2@Ge_{16}]^{4-}$: Localized versus Delocalized Bonding in Two Isomeric Intermetalloid Clusters. *Chem. - Eur. J.* **2018**, *24*, 699−705.

(19) Esenturk, E. N.; Fettinger, J. C.; Eichhorn, B. W. Synthesis, Structure, and Dynamic Properties of $[Ni_2Sn_{17}]^{4-}$. *J. Am. Chem. Soc.* **2006**, *128*, 12−13.

(20) Kesanli, B.; Halsig, J. E.; Zavalij, P.; Fettinger, J. C.; Lam, Y. F.; Eichhorn, B. W. Cluster Growth and Fragmentation in the Highly Fluxional Platinum Derivatives of $Sn_9^{4-}$: Synthesis, Characterization, and Solution Dynamics of $Pt_2@Sn_{17}^{4-}$ and $Pt@Sn_9H_3$. *J. Am. Chem. Soc.* **2007**, *129*, 4567−4574.

(21) (a) Hlukhyy, V.; He, H. Y.; Jantke, L. A.; Fässler, T. F. The Neat Ternary Solid $K_{5-x}Co_{1-x}Sn_9$ with Endohedral $[Co@Sn_9]^{5-}$ Cluster Units: A Precursor for Soluble Intermetalloid $[Co_2@Sn_{17}]^{5-}$ Clusters. *Chem. - Eur. J.* **2012**, *18*, 12000−12007. (b) He, H. Y.; Klein, W.; Jantke, L. A.; Fässler, T. F. Metal-Centered Zintl Ions Isolated by Direct Extraction from Endohedral Intermetallic Precursor: $[Co_{1-x}@Sn_9]^{4-}$ ($x \approx 0.32$) and $[Co_2@Sn_{17}]^{5-}$. *Z. Anorg. Allg. Chem.* **2014**, *640*, 2864−2870.

(22) (a) Sun, Z.-M.; Xiao, H.; Li, J.; Wang, L. S. $Pd_2@Sn_{18}^{4-}$: Fusion of Two Endohedral Stannaspherenes. *J. Am. Chem. Soc.* **2007**, *129*, 9560−9561. (b) Kocak, F. S.; Zavalij, P.; Lam, Y. F.; Eichhorn, B. W. Solution Dynamics and Gas-phase Chemistry of $Pd_2@Sn_{18}^{4-}$. *Inorg. Chem.* **2008**, *47*, 3515−3520. (c) Goicoechea, J. M.; Sevov, S. C. $[(Pd\text{-}Pd)@Ge_{18}]^{4-}$: A Palladium Dimer Inside the Largest Single-Cage Deltahedron. *J. Am. Chem. Soc.* **2005**, *127*, 7676−7677.

(23) Goicoechea, J. M.; Sevov, S. C. $[(Ni\text{-}Ni\text{-}Ni)@(Ge_9)_2]^{4-}$: A Linear Triatomic Nickel Filament Enclosed in a Dimer of Nine-Atom Germanium Clusters. *Angew. Chem., Int. Ed.* **2005**, *44*, 4026−4028.

(24) Lips, F.; Clérac, R.; Dehnen, S. $[Pd_3Sn_8Bi_6]^{4-}$: A 14-Vertex Sn/Bi Cluster Embedding a $Pd_3$ Triangle. *J. Am. Chem. Soc.* **2011**, *133*, 14168−14171.

(25) (a) Peters, B.; Lichtenberger, N.; Dornsiepen, E.; Dehnen, S. Current Advances in Tin Cluster Chemistry. *Chem. Sci.* **2020**, *11*, 16−

26. (b) Wilson, R. J.; Lichtenberger, N.; Weinert, B.; Dehnen, S. Intermetalloid and Heterometallic Clusters Combining p-Block (Semi)Metals with d- or f-Block Metals. *Chem. Rev.* **2019**, *119*, 8506−8554.
(26) Stegmaier, S.; Fässler, T. F. A Bronze Matryoshka: The Discrete Intermetalloid Cluster $[Sn@Cu_{12}@Sn_{20}]^{12-}$ in the Ternary Phases $A_{12}Cu_{12}Sn_{21}$ (A = Na, K). *J. Am. Chem. Soc.* **2011**, *133*, 19758−19768.
(27) Schmid, G. Large clusters and colloids. Metals in the Embryonic State. *Chem. Rev.* **1992**, *92*, 1709−1727.
(28) (a) Banh, H.; Hornung, J.; Kratz, T.; Gemel, C.; Pothig, A.; Gam, F.; Kahlal, S.; Saillard, J.-Y.; Fischer, R. A. Embryonic Brass: Pseudo Two Electron Cu/Zn Clusters. *Chem. Sci.* **2018**, *9*, 8906−8913. (b) Freitag, K.; Gemel, C.; Jerabek, P.; Oppel, I. M.; Seidel, R.; Frenking, G.; Banh, H.; Dilchert, K.; Fischer, R. A. The σ-Aromatic Clusters $[Zn_3]^+$ and $[Zn_2Cu]$: Embryonic Brass. *Angew. Chem., Int. Ed.* **2015**, *54*, 4370−4374.
(29) Meyer, E. M.; Gambarotta, S.; Floriani, C.; Chiesi-Villa, A.; Guastini, C. Polynuclear Aryl Derivatives of Group 11 Metals. Synthesis, Solid State-solution Structural Relationship, and Reactivity with Phosphines. *Organometallics* **1989**, *8*, 1067−1079.
(30) Wang, Z. C.; Tkachenko, N. V.; Qiao, L.; Matito, E.; Muñoz-Castro, A.; Boldyrev, A. I.; Sun, Z.-M. All-metal σ-antiaromaticity in Dimeric Cluster Anion $\{[CuGe_9Mes]_2\}^{4-}$. *Chem. Commun.* **2020**, *56*, 6583−6586.
(31) (a) Wilson, R. J.; Broeckaert, L.; Spitzer, F.; Weigend, F.; Dehnen, S. $\{[CuSn_5Sb_3]^{2-}\}_2$: A Dimer of Inhomogeneous Superatoms. *Angew. Chem., Int. Ed.* **2016**, *55*, 11775−11780. (b) Geitner, F. S.; Klein, W.; Fässler, T. F. Formation of the Intermetalloid Cluster $[AgSn_{18}]^{7-}$ − the Reactivity of Coinage Metal NHC Compounds towards $[Sn_9]^{4-}$. *Dalton Trans.* **2017**, *46*, 5796−5800. (c) Pani, M.; Merlo, F.; Fornasini, M. L. Intermetallic Phases in the Ca-Cu-Sn System. *Z. Anorg. Allg. Chem.* **2007**, *633*, 1581−1586. (d) Sun, Z.-M.; Xia, S. Q.; Huang, Y. Z.; Wu, L. M.; Mao, J. G. $Ca_6Cu_2Sn_7$: Novel 3D Open Framework with Unusual $Sn_4$ Tetramers. *Inorg. Chem.* **2005**, *44*, 9242−9246.
(32) Ziegler, T. Approximate Density Functional Theory as a Practical Tool in Molecular Energetics and Dynamics. *Chem. Rev.* **1991**, *91*, 651−667.
(33) *ADF2019.103*; SCM: Amsterdam, 2019; http://www.scm.com.
(34) te Velde, G.; Bickelhaupt, F. M.; Baerends, E. J.; Fonseca-Guerra, C.; van Gisbergen, S. J. A.; Snijders, J. G.; Ziegler, T. Chemistry with ADF. *J. Comput. Chem.* **2001**, *22*, 931−967.
(35) Perdew, J. P.; Burke, K.; Ernzerhof, M. Generalized Gradient Approximation made simple. *Phys. Rev. Lett.* **1996**, *77*, 3865−3868.
(36) McGrady, J. E. A Unified Approach to Electron Counting in Main-Group Clusters. *J. Chem. Educ.* **2004**, *81*, 733−737.
(37) Mitzinger, S.; Broeckaert, L.; Massa, W.; Weigend, F.; Dehnen, S. Understanding of multi-metallic cluster growth. *Nat. Commun.* **2016**, *7*, 10480.



https://dx.doi.org/10.1021/jacs.0c04815
*J. Am. Chem. Soc.* 2020, 142, 13288−13293